Structurally stitched woven preforms: experimental characterisation, geometrical modelling, and FE analysis

V. Koissin[1], J. Kustermans[1], S. V. Lomov*[1], I. Verpoest[1], H. Nakai[2], T. Kurashiki[2], K. Hamada[2], Y. Momoji[2] and M. Zako[2]

In this study, experimental data, geometrical models, and finite element analysis are presented for typical structurally stitched multilayer preform composed of quasi-unidirectional carbon fibre woven fabric. The term 'structural' presumes here that the stitching yarn does not only consolidate the plies (as the non-structural one does) but forms also a through the thickness reinforcement. One stitching technique, tufting, is studied, with 67 tex carbon yarn. The models account for general features of the local preform geometry and are believed to allow for a sufficient modelling on the mesoscale (textile unit cell) level. Experimental and theoretical results are presented, compared and discussed; a 'road' map is proposed for the modelling of structurally stitched preforms.

Keywords: Textile composite, Structural stitching, Experimental characterisation, Modelling, Finite element analysis

Introduction

It is well known that a significant variability can exist in the internal geometry of a textile composite.[1] Particularly, this is the case for the structurally stitched preforms. The fibre placement is not uniform even in a raw material (fibre tows or yarns). Then, the needles of a knitting device (for non-crimp fabrics (NCFs)) or a textile process still increase this non-uniformity of the fibre content. While stitching structurally (i.e. with a relatively thick and firm yarn), the fibres are again pushed aside the needle; a breakage and vertical movement (crimpling) of some fibres can also be induced.[2] During the forming and compression in a mould, the fibre distribution is changed again. Finally, the micro- and mesostructure of a composite part can differ very much from that of the raw fabric.

Variability of the internal structure includes also random nesting of layers, random overlap of the 'structural' and 'non-structural' piercing patterns and openings (for NCF's), wide distribution of the opening dimensions, etc.[2,3] As a result, the composite has a complex hierarchical (meso- and micro-) structure having a significant randomisation. The mesolevel (0·1–100 mm) includes the yarn loops (non-structural and structural), openings in the fibrous plies, gaps between the plies, etc. The microlevel (10–100 μm) embraces the variable fibre content in a ply and yarn. Then, an investigation is difficult due to a bulk of parameters (stitching method/speed, distance between stitches/seams, dimension of the needle, properties of the preform/yarn, yarn tension, etc.). The modelling is thus sophisticated and case dependent, and a broad experience is required.

The present study aims at a generalised mesoscale modelling approach suitable for the engineering purposes. The focus is laid on theoretical (method of inclusions) and finite element (FE) estimation of the homogenised mechanical properties. Damage onset is also considered.

Materials

Quasi-unidirectional hybrid woven fabric (warp: 24 K carbon tows alternated with thin polysulfone yarns; weft: the same polysulfone yarns) with the total areal weight of 226 g m^{-2} is used as the raw material (Fig. 1). The areal weight of the carbon tows is 200 g m^{-2}.

To characterise the mesogeometry, the fabric surface is scanned, and $\sim$50 lines are marked in a separate image layer for each dimension (yarn width, spacing). The layer is saved as a bitmap file and committed to a Matlab applet, which searches for the marked lines and calculates their lengths. Finally, the average values and standard deviations are assessed. For the carbon tows, the measured width is $4{\cdot}34 \pm 0{\cdot}14$ mm that agrees well with the manufacturer's data,[4] $6 \pm 0{\cdot}5$ ends per inch or 4·23 mm. For the polysulfone yarn, the measured width is $0{\cdot}22 \pm 0{\cdot}0$ mm (warp) or $0{\cdot}91 \pm 0{\cdot}18$ mm (weft) that also agrees well with the datasheet ($6 \pm 0{\cdot}5$ ends or 6 ± 1 picks per inch).

The fabric is composed of 28 plies having symmetric stacking sequence (90°/45°/0°/0°/−45°/90°/−45°/0°/0°/

[1]Department of Metallurgy and Materials Engineering, Katholieke Universiteit Leuven, Kasteelpark Arenberg 44, B 3001 Heverlee, Belgium
[2]Graduate School of Engineering, Osaka University, 2-1 Yamadaoka, Suita, Osaka 565-0871, Japan

*Corresponding author, email Stepan.Lomov@mtm.kuleuven.be

Published by Maney on behalf of the Institute
Received 8 September 2008; accepted
DOI 10.1179/174328909X387865

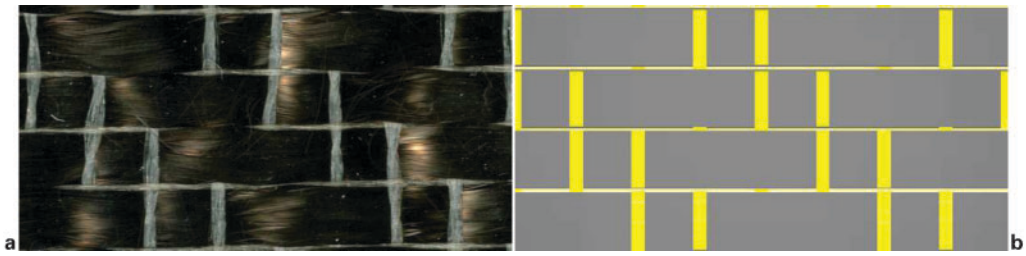

1 *a* woven fabric and *b* its geometrical model built using WiseTex

2 *a* face side and *b* backside of stitched preform

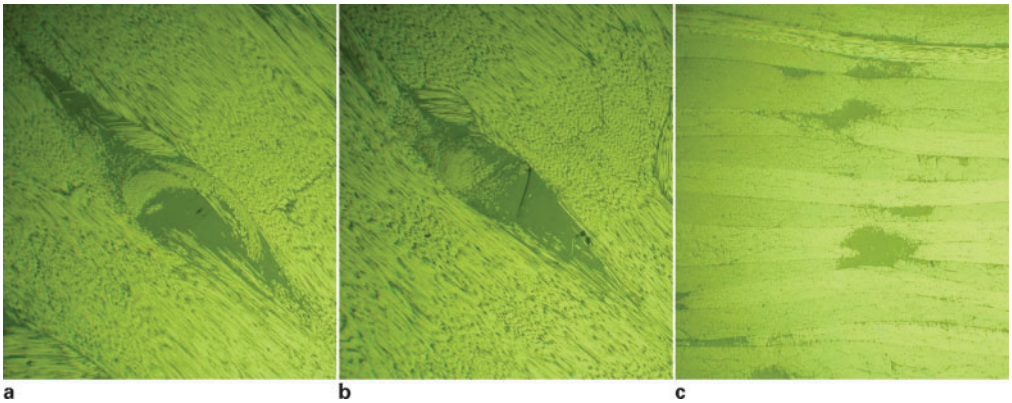

3 Typical micrographs of *a* in plane, *b* in plane (layer 5) or *c* cross-sections

$45°/0°/-45°/0°/45°)_s$, where 90° corresponds to the warp (carbon fibre) direction in the surface plies, i.e. to the horizontal direction in Fig. 1.

For the structural stitching, 1 K carbon yarn[5] and tufting method (KL RS 522 stitching head mounted on a KUKA robot) are employed. The machine direction coincides with 0° direction of the preform. The piercing pattern is square 5×5 mm; the backside loop height is also ~ 5 mm. Typical photos of the stitched preform are shown in Fig. 2.

During the tufting, fibre free zones (called 'openings') appear around the stitching sites; these openings are naturally oriented along the global fibre orientation in the ply. Their geometrical characterisation is performed in the same way as described above for the fabric structure; results are given in Table 1. Since the backside openings almost hide under numerous yarn loops (Fig. 2*b*), they are cut off within a small area sufficient for the measurements. The backside loops show a relatively wide distribution in width and height; this is obviously due to the fact that these parameters are hardly controlled during the tufting and much influenced by a friction between the plies and yarn.

Composite plates (stitched and non-stitched) are manufactured using the liquid resin (toughened epoxy) infusion. The final thickness is 5·32 mm that gives the average fibre volume fraction V_f of 58% (without taking openings into account). Several pieces are inspected with an optical microscope for details of the internal structure. Typical micrographs of the stitching sites are shown in Fig. 3*a*. Measured dimensions are listed in Table 1, which reveals significant ($\sim 50\%$) reduction in the size of the openings if compare with the dry preform. This effect should be attributed to severe densification of

Table 1 Measured dimensions of 'openings' and stitching yarn

Preform	Length, mm	Width, mm	Length/width ratio	Stitching yarn width, mm	Loop height, mm	Loop width, mm
Dry, face	6·95±1·21	1·42±0·17	4·88	1·09±0·28	–	–
Dry, back	6·60±1·19	0·74±0·11	8·92	0·87±0·18	5·00±0·81	3·61±0·54
Cured, face	3·71±0·77	0·84±0·13	4·42	–	–	–
Cured, inner	3·56±0·79	0·87±0·16	4·10	–	–	–
Cured, back	3·95±0·79	0·81±0·25	4·88	0·85±0·23	4·87±0·85	3·22±0·39

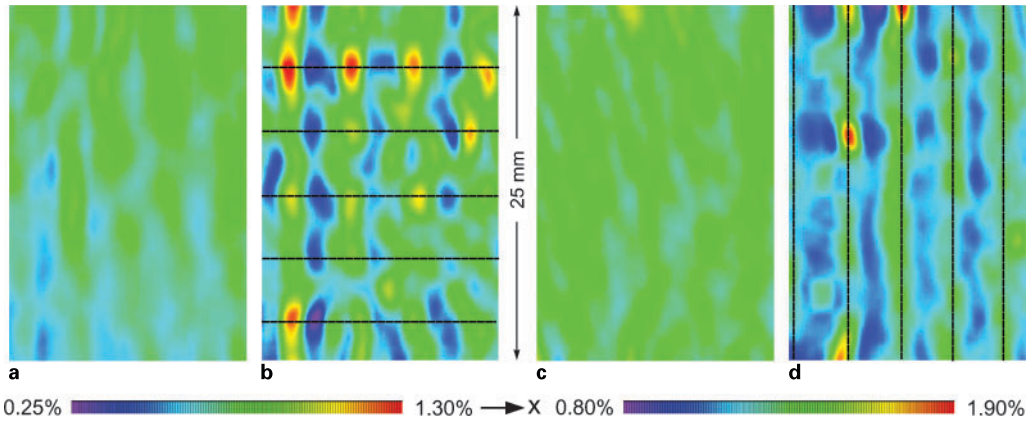

a, *c* virgin; *b*, *d* stitched, face

4 Surface strains ε_x under loading in *a*, *b* 0° and *c*, *d* 90° directions: load is applied in *x* direction; average strain level is 0·75 or 1·35%, respectively; presumable positions of stitching yarns are shown with black lines

the fibrous plies in the mould (thickness in the dry state is ~9 mm). Taking an average rhomboid 3·6 × 0·9 mm opening, it can be estimated that V_f in plies after the stitching is 62%, and the openings occupy 6·5% of the total volume.

The widths of the inner and surface openings are almost the same. This disagrees with other materials[2] which show wider surface openings, since the yarn loop bends at the face and backside and, therefore, pushes away the fibres more than in the inner plies. In the present case the small difference can be due to severe compression in the mould.

A prominent nesting of the plies can be observed in Fig. 3*c*, where the ply waviness amplitude sometimes exceeds the average ply thickness (5·32/28=0·19 mm). This effect should also be attributed to the out of plane compression in the mould.

In the impregnated state, the yarn loop width at the face side is not measured due to roughness of this surface; a smooth surface appears only after polishing out a relatively thick layer including almost all yarn material. As for the backside, it is interesting that the moulding changes the yarn width not very much, probably due to its twist.

The material properties, Young's modulus E, Poisson's ratio ν (theoretically estimated for the transversal direction), ultimate tensile stress σ_{ult}, etc., are listed in Table 2.

Experimental

Uniaxial tensile tests are performed according to ASTM D3039; i.e. specimens having a constant 5·32 × 30 mm cross-section are used. Series of 6 specimens are tested for 0° (along the structural stitching) and 90° directions, at the crosshead displacement rate of 3 mm min^{-1}. The tests are monitored with the acoustic emission (AE) and full field strain registrations. Since the AE sensors should be removed before the specimen failure, the loading is not completely monotonical but is paused at a certain load level.

Figure 4 shows typical strain fields at the face side of different specimens. It is seen that the tufting causes prominent strain concentrations at the stitching sites, in comparison with the non-stitched specimens. For some specimens loaded in 90° direction, analysis of the strain history in such local maximums reveals almost constant strain rate until a moment, when it starts to increase rapidly. This moment can be attributed to the damage onset; afterwards, the local strain more and more differs from the average one. For example, the specimen shown in Fig. 4*c* and *d* fails at the average strain of 1·57%, while the ultimate local strain approaches 2·5%; the rapid increase starts at ~1·1% of the average strain (the stress level of ~400 MPa). However, it is difficult to say if it is the damage driving the final failure or not; an X-ray investigation could clarify this.

Figure 5*b* and *c* shows the cumulative energy of events recorded with the AE equipment. The damage onset is seen already at the beginning of the tests, when a few low energy events occur with low frequency. At a certain moment, the frequency increases, the energy content rises quickly, and the specimens starts to emit popping sounds indicating appearance of relatively large cracks (since this occurs at different stresses for 0° and 90° specimens, the sounds are not due to a tab cracking). This should be attributed to a mass microcrack formation, presumably in the off axis plies; corresponding stress level is denoted further as σ^{dam}. Under 0° loading, this mass cracking starts at the stress level of ~160 MPa both for the non-stitched and stitched specimens, while for 90° loading the stress levels differ significantly (250 versus 120 MPa).

The clearest picture of the material behaviour is given by the cumulative sum of AE event counts (Fig. 5*c*). A drastic change of the curve slope is seen at σ^{dam} level. It

Table 2 Properties of composite constituents: longitudinal/transversal

	Material	Fibre Φ, μm	Twist, t m^{-1}	Density, g cm^{-3}	Lin.dens, tex	*E*, GPa	ν	σ_{ult}^{tens}, MPa
Ply	Tenax IMS 5131	5	0	1·80	820	290/14	0·236/0·011	5600/–
Ply	Priform ST54/2Z	30	Z2	1·24	54	2·48	0·3	70·2
Stitch	Tenax HTA 5241	7	S15	1·76	67	238/14	0·230/0·014	3950/–
Resin	Cycom 977-2	–	–	1·31	–	3·52	0·3	81·4

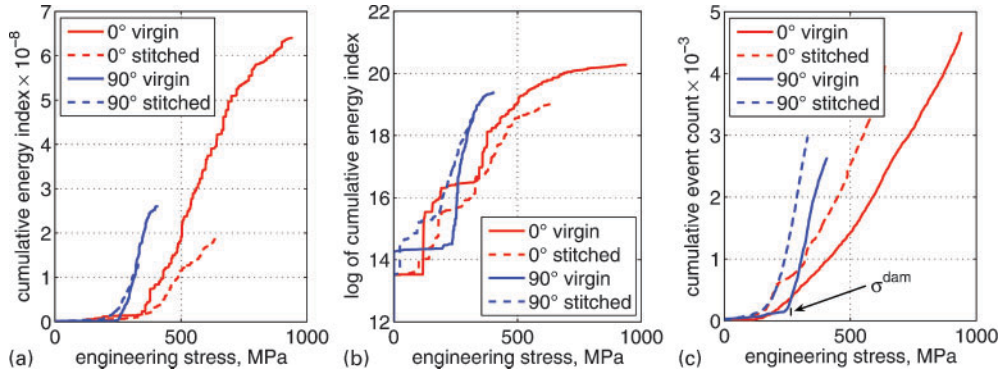

5 Acoustic emission energy in *a* normal and *b* logarithmic scales, *c* cumulative sum of AE event counts

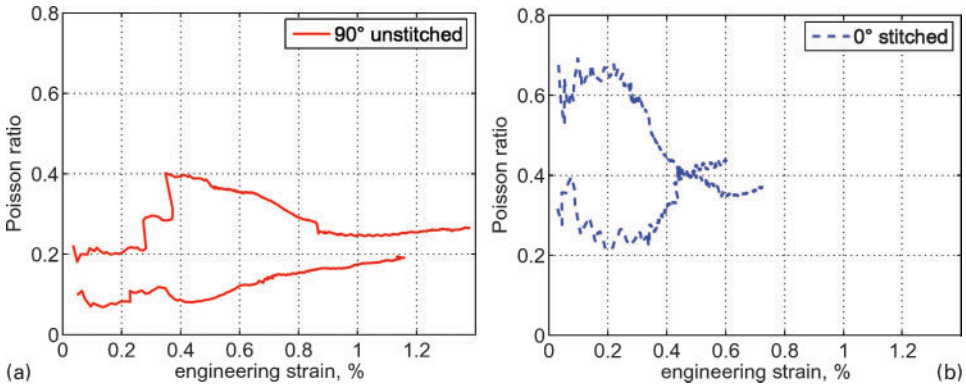

a 90° unstitched; *b* 0° stitched

6 Poisson's ratio variation during loading

is also interesting to note that the event curves have two almost linear parts; this means that the increase in the event number is almost constant within each part.

Similar behaviour is observed for the Poisson's ratio (Fig. 6), which also shows a distinct change at about the same transition strain as the AE curves ($\varepsilon_0^{dam} = 0{\cdot}2\%$, $\varepsilon_{90}^{dam} = 0{\cdot}5/0{\cdot}3\%$). Before this threshold, the plots show a wide variation; its reason is still not clear for the authors. After passing the threshold, the Poisson's ratio is more conformable within each test series and keeps almost constant magnitude as the axial strain increases.

Table 3 summarises the measured mechanical properties: the Poisson's ratios (averaged in the strain range 0·05–0·3%) and Young's moduli, as well as σ^{dam} level (Fig. 5*c*). The standard deviations do not exceed 15%.

Geometrical modelling

The preform model is built using StitchTex software, which is a stand alone application based on WiseTex approach to the generalised textile description.[6] Thus, StitchTex is integrated with existing geometrical and mechanical models of relaxed or deformed two- and three-dimensional woven, two and three axial braided, weft knitted, and non-crimp warp knit stitched fabrics, and laminates built on their base. The integration with WiseTex allows also for a direct use of the existing software solutions for the modelling of a resin flow through the reinforcement, micromechanical calculations of the composite properties, micro–macro analysis of a composite part, FE models, and virtual reality visualisation.[6]

The present model is an inevitable simplification of the actual internal structure; e.g. it does not account neither for heavy nesting nor for deplanation of the plies caused by consolidation in the mould (Fig. 3*c*). It is obvious that a semianalytical approach can not mimic such features, which are hardly modelled even in an FE analysis.

First, consider the fabric model, which is built with the thickness of 0·19 mm (the laminate thickness divided by 28 plies) and parameters listed in the section on 'Materials'. To achieve the best agreement with the nominal total areal weight of the fabric, a denser structure is modelled for the carbon yarns (0·117 × 3·9 mm cross-section). The polysulfone yarn width is also accepted a little smaller than the measured one: the cross-sectional size is 0·115 × 0·19 mm (along carbon yarns) or 0·024 × 0·9 mm (across them).

The model is built easily with WiseTex but absence of nesting results in a too high local V_f inside the yarns; it even slightly exceeds 100% (in reality these 'excess' fibres fill the voids between the yarns and plies due to nesting

Table 3 Homogenised mechanical properties of composite (mean values, non-stitched/stitched): moduli are given in GPa, stress in MPa

	E_0	E_{90}	E_z	$G_{0,90}$	$\nu_{0,90}$	$\nu_{90,0}$	σ_0^{dam}	σ_{90}^{dam}
Test data	73·4/87·7	46·9/38·9	–	–	0·271/0·353	0·249/0·161	148/174	247/120
TexComp	93·6/94·5	49·6/50·2	7·5/8·6	24·0/24·2	0·338/0·337	0·179/0·179	–	–
FE	88·9/86·2	46·3/44·7	8·0/8·5	21·8/21·2	0·368/0·374	0·192/0·194	–/165	–/140

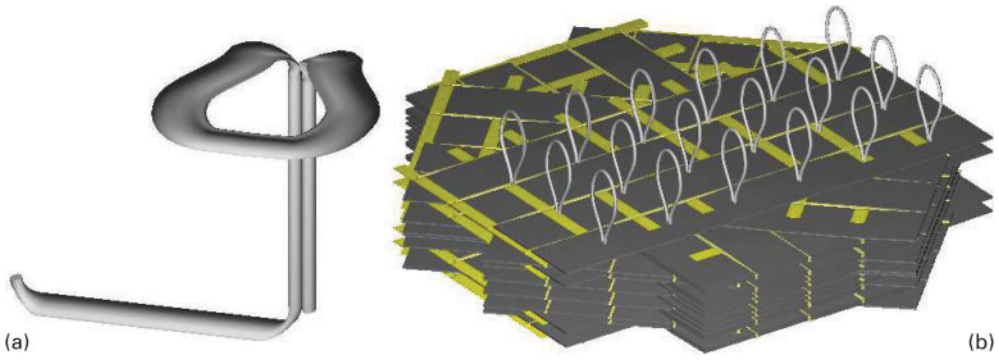

7 Models of *a* stitching loop repeat and *b* stitched preform

and distortion of the yarn shapes). If, other way round, the yarn thicknesses are chosen to give a reasonable V_f, then the ply thickness is overestimated, and the overall V_f is underestimated. Since the correct V_f is crucial for the method of inclusions used further to calculate the homogenised stiffness matrix, the latter way (with a realistic V_f inside yarns) is adopted. Then, the geometrical model is created with the thickness slightly larger than the nominal one and local V_f of $\sim$90% (below the ultimate packing case of 90·7%) inside the yarns. The warp and weft crimp is chosen to minimise the fabric thickness for the given yarn dimensions. The model of the reinforcement fabric is shown in Fig. 1*b*.

The preform model is built by:

(i) multiplication and rotation of the ready fabric model exported from WiseTex and
(ii) appending the stitching loops (optionally).

The following simplifying assumptions are accepted to produce a physically sound and computationally feasible model sufficient for a correct estimation of the homogenised properties:

(i) as already noticed above, no nesting is modelled. The preform is a stack of flat plies, which have equal uniform thickness, and their bounding boxes do not intersect
(ii) the openings are not modelled, since: (a) WiseTex approach does not allow to split a yarn and (b) the openings have a negligible effect on the homogenised stiffness.[7] Thus, there are interpenetrations of the stitching and fabric yarns but this does not matter for the method of inclusions used further
(iii) the piercing pattern is regular (constant stitching length and distance between seams). This is a reasonable simplification for a well controlled robot process, although some irregular scatter can be observed even in such an 'ideal' case[2,3]
(iv) seams are straight (no zigzag offset of the piercing pattern) and parallel. No initial shift is assumed between them (i.e. a rectangular piercing pattern is produced)
(v) the stitching yarn consists of a single strand (in reality, it can be composed of several twisted strands). This assumption is accepted due to a strong randomisation of the strand positions and shapes along the yarn path[2]
(vi) the cross-section is circular along the through the thickness yarn path. The yarn flattening is optionally modelled only at the preform surface, to avoid segmentation of the surface plies in an FE model (since the yarn diameter can exceed the ply thickness, and the ply can be cut if the yarn is sunk into the preform). The cross-sectional area is preserved constant along the yarn (just to simplify the FE model)
(vii) the through the thickness yarn path is either straight or helical (spiral built around an imaginary straight line). In reality, it can be inclined due to a local deformation of the preform during the stitching, draping, compression in the mould, etc. This can play a role for the out of plane stiffness but is difficult to be accounted for without an unnecessary complication of the model
(viii) elastic yarn bending is assumed in some cases; in other cases, the yarn bent shape is defined reasoning from purely geometric considerations (straight lines, arches)
(ix) the backside loops are placed regularly. Their height is equal and a little reduced if compare with the measured one. This allows avoiding interpenetrations of the stitching yarns that is important for the FE model discussed in the section on 'finite element modelling'.

The geometrical models of the stitching loop and stitched preform are shown in Fig. 7. In the latter case, for better visualisation, the stitching loops are not sunk and flattened.

To calculate the homogenised elastic properties, the method of inclusions[8] is used, which is implemented in TexComp software. In the computational scheme, the model thickness is reduced artificially to achieve the nominal one (5·32 mm), thus 'nesting' the inclusions into the volume having the correct average V_f.

Results are listed in Table 3 and are in a good agreement with the experimental data. The difference can be due to natural reasons:

(i) inaccuracy in the material properties (which can differ a little from the nominal values) and
(ii) neglected deplanation and nesting of the plies. There is also an error inherent for the homogenisation procedure; particularly, it assumes no free surfaces, while the laminate thickness is limited.

Finite element modelling

The mesolevel FE analysis (meshing of the laminate and stitching yarn volumes, mesh superposition technique) is performed using MeshTex/Sacom/M3 softwares.[9]

To decrease the computational costs, it is interesting to assess the influence of the stitching yarn and openings on the FE results; the stitching loop is quite complex, and if it is possible to obtain reasonable estimations of

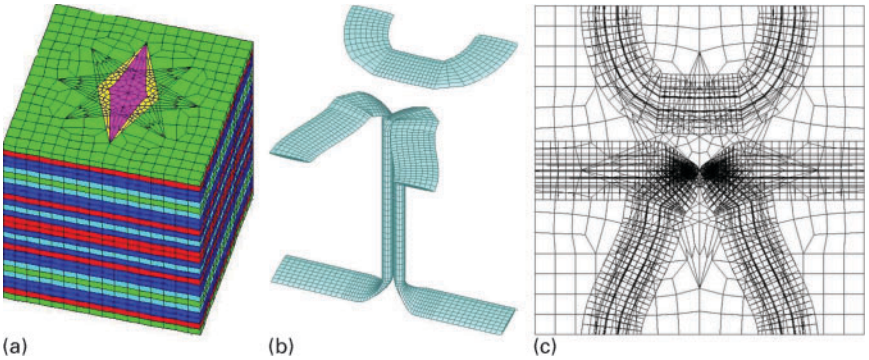

8 Finite element mesh of laminate and stitching loop (5312 elements in total): for backside ply, opening is shown in pink, and area of reoriented fibres in yellow

the composite properties without the stitching included, e.g. as conducted in Ref. 10, then preprocessing of the FE model can be much easier.

Thus, the FE analysis is performed for several models of different complexity: (A) only laminate without stitching and openings, (B) with openings but without fibre deviation around them and without stitching, (C) the same with fibre deviation, and (D) with stitching and openings. In the last two variants, the local fibre reorientation around the openings is accounted for, following the procedure proposed in Ref. 7. Both the opening and the area of misaligned fibres are modelled as ideally rhomboidal.

For simplicity, textile structure of the plies is neglected, and they are modelled as unidirectional mats having the same average V_f of the carbon fibres as the initial fabric. This is a reasonable simplification due to compact placement and low crimp of the carbon fibre tows in the relaxed fabric. Polysulfone yarns are not modelled also, since their stiffness and strength are similar to these of the matrix material (Table 2). The homogenised orthotropic properties are determined using the Chamis' formulae (Table 4).

The stitching loop is meshed using the centerline coordinates and cross-sections imported from StitchTex geometrical model described above (Fig. 7*a*). As noticed in the section on 'Geometrical modelling', the cross-sectional area is preserved to be constant along the stitching loop, and only the shape changes (ellipse with different axes ratio).

The FE models of the laminate and stitching loop are shown in Fig. 8. To fit $5 \times 5 \times 5{\cdot}32$ mm unit cell, the backside loop of the stitching yarn is meshed in two parts. Periodic boundary conditions (translation symmetry of the unit cell) are applied in the model plane.

To obtain the elastic properties, the model is sequentially loaded in 0°, 90°, and z directions by applying 0·1% tensile strain. Results are given in Table 5; in Table 3, selected results are compared with the test data and theoretically estimated values; they are in a good agreement. Typical stress distributions are shown in Fig. 9. It is seen that the opening results in a prominent disturbance of the stress field; introduction of the stitching loop causes even greater stress concentrations. However, the effect on the stiffness matrix is very small, less than 3%. The exception is the out of plane stiffness, which rises in 7% if the stitching loop is superimposed.

The damage onset and propagation are calculated also, using the Hoffman criterion; the damage mode is set by the maximum value among the corresponding stress to strength ratios. The strength properties of each material (stitching yarn, ply with or without openings) are estimated using the Rosen's model. It is obtained from Table 5 that the opening, local fibre reorientation, and stitching loop trigger the damage onset, which appears earlier than in the case of plane laminate (model A). Evolution of the model provokes also the damage localisation (Table 6) which is naturally absent in model A. In models B and C the initial damage concentrates around the opening, at that the fibre deviation results not only in earlier damage occurrence but also in the new set of its locations under the in plane loading. After introducing the stitching loop (model D), the damage positions stay the same under loading in 90° direction, while further localisation occurs when the tension is applied in 0° direction. When the model is loaded in the transversal direction, the damage localises also, contrary to models A–C, where it occurs simultaneously in all layers. The damage onset stresses are given in Table 3

Table 4 Material properties estimated using Chamis' formulae: moduli are in GPa

	V_f, %	E_L	E_T	E_Z	G_{LT}	G_{TZ}	G_{ZL}	ν_{LT}	ν_{TZ}	ν_{ZL}
Ply, no openings	58	168·5	8·6	7·2	5·7	2·3	2·8	0·255	0·373	0·012
Ply, with openings	62·1	180·0	9·0	7·5	6·0	2·5	3·0	0·253	0·361	0·013
Stitching yarn	90·7	216·0	11·7	11·7	73·3	4·7	73·3	0·234	0·237	0·013

Table 5 Estimated mechanical properties: moduli are in GPa, strains are in %

	Opening	Fibre dev.	Stitching	E_0	E_{90}	E_z	ε_0	ε_{90}	ε_z
Model A	−	−	−	88·89	46·30	7·99	0·8	0·8	1·0
Model B	+	−	−	84·98	44·50	7·98	0·4	0·4	0·8
Model C	+	+	−	85·74	44·91	7·99	0·3	0·3	0·8
Model D	+	+	+	86·19	44·66	8·52	0·2	0·3	0·4

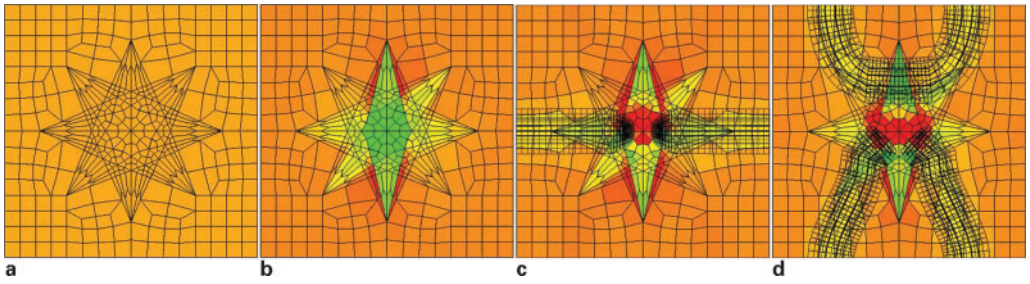

a model A; *b* models B and C; *c* model D, face; *d* model D, back

9 Typical stress distributions σ_z under *z* loading at 0·1% average strain

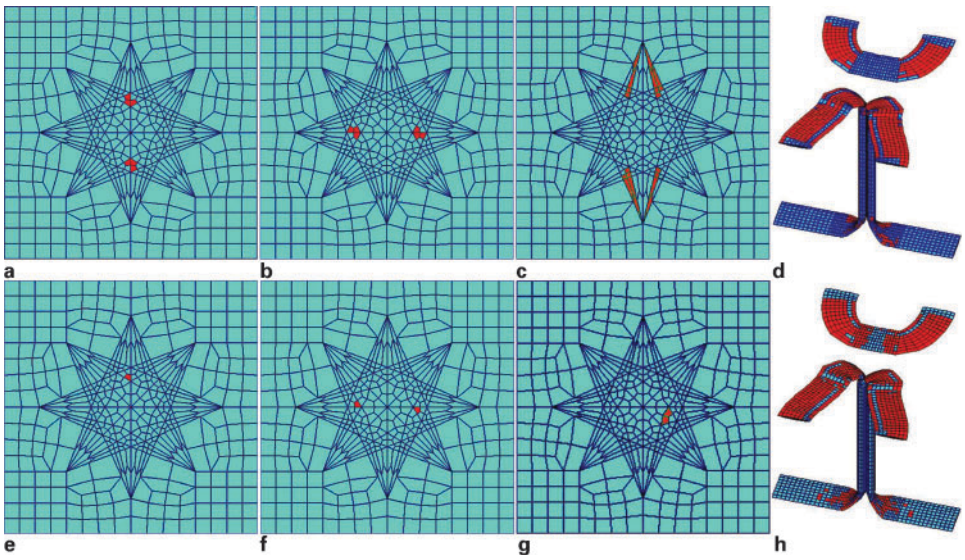

a, *e* load 0°, mode T< *b*, *f* load 90°, mode T< *c*, *g* load Z, mode Z&ZL; *d*, *h* load 0°, mode; T&LT

10 Damage onset in *a–c* models B and C and *e–g* model D: backside, average strains are listed in Table 5, *d*, *h* damage in yarn loop at 0·1% average strain: dark areas are damaged elements

for models A and D and are in a good agreement with the test data.

Typical damage onset positions are shown in Fig. 10. This figure illustrates also the damage propagation in the stitching loop; its elements reach the ultimate state much earlier than the ply elements, obviously due to a complex load flow in the loop and its underestimated (due to adopted V_f of 90·7%) transversal strength.

The damage growth also depends on the model complexity. For example, Fig. 11 gives a comparison between the damage propagation in models B and C. It is seen that the fibre reorientation results in a distinct change of the damage growth direction. If the fibre deviation is not modelled, the damage propagates across the openings; otherwise, it spreads lengthwise. The damage is also more extensive as revealed by Fig. 12, at that at the face side the damage zone coincides with the stitching loop position.

Conclusions

This paper deals with a case study of the mesolevel geometrical and FE modelling of a structurally stitched woven laminate. The main results are as follows.

1. The structural stitching produces a negligible influence on the in plane components of the homogenised stiffness matrix; this observation corresponds to earlier results by other authors, e.g. Ref. 11. Accounting

Table 6 Damage onset in plies (0°, 90° loading – T & LT mode; *z* – Z & ZL mode)

Ply		90°	45°	0°	°0	−45°	90°	−45°	0°	0°	45°	0°	−45°	0°	45°
Model A	0°, 90°	−	+	−	−	+	−	+	−	−	+	−	+	−	+
	z	+	+	+	+	+	+	+	+	+	+	+	+	+	+
Model B	0°	−	+	+	+	+	−	+	+	+	+	−	+	−	+
	90°	+	+	−	−	+	+	+	−	−	+	−	+	−	+
	z	+	+	+	+	+	+	+	+	+	+	+	+	+	+
Model C	0°	−	−	+	+	−	−	−	+	+	+	−	+	−	+
	90°	+	−	−	−	−	−	−	−	−	−	−	−	−	+
	z	+	+	+	+	+	+	+	+	+	+	+	+	+	+
Model D	0°	−	−	+*	−	−	−	−	−	−	−	−	−	−	−
	90°	+	−	−	−	−	−	−	−	−	−	−	−	−	+
	z	+†	−	−	−	−	−	−	−	−	−	−	−	−	−

*Damage initiates at 0·2% in the face side only; further at 0·3% it spreads to the same layers as in model B.
†Occurs at the backside only.

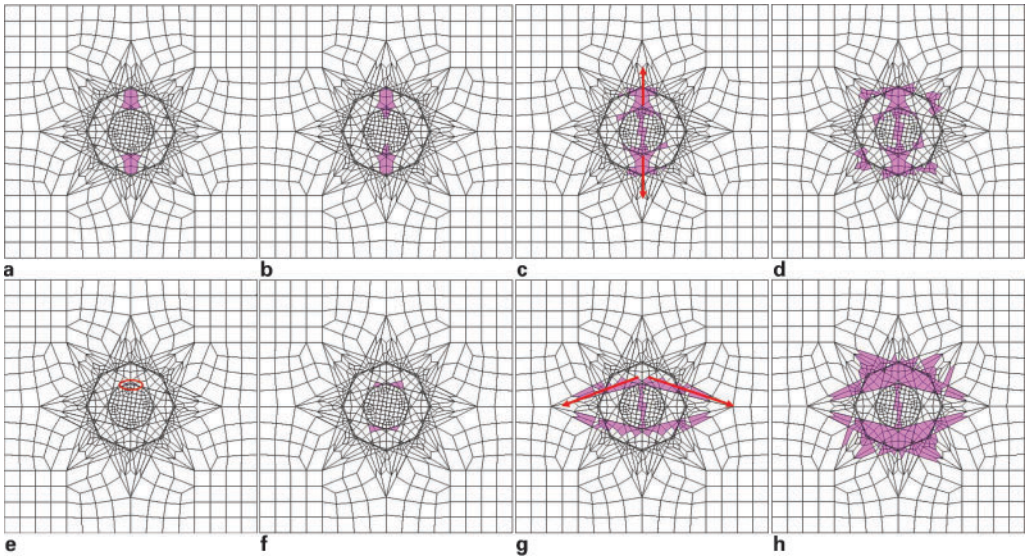

a, *e* 0·2% strain; *b*, *f* 0·4% strain; *c*, *g* 0·7% strain; *d*, *h* 0·8% strain

11 Damage propagation in 0° layer in *a–d* model B and *e–h* model C under loading in 0° direction: mode T&LT, marked pink

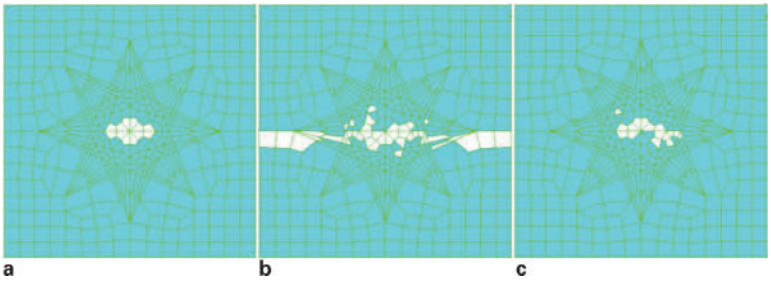

a model A; *b* model D, face; *c* model D, back

12 Damaged elements in surface plies (mode L, marked white) under loading in 90° direction at 0·8% average strain

for the stitching loop is important only for the transversal stiffness and related constants. Thus, relatively simple models without openings can be used to obtain the stiffness matrix. To account for the through the thickness reinforcement, the simplest 'pin like' model of the stitching can be sufficient, instead of a detailed modelling of the complex loop shape.

2. However, the stress–strain fields are sensitive to the local geometry, which can play the role of a stress concentrator and trigger damage. Therefore, presence of the stitching yarn and openings, as well as specifics of their modelling is important for a correct computation of the damage onset and propagation. Of course, word 'correct' should be understood here in a relative sense due to a strong randomisation of the micro- and mesolevel internal structure of a real composite.

3. For a typical structurally stitched composite, theoretical estimations (method of inclusions) and results of the FE simulation are compared with experimentally measured properties. They agree well thus showing efficiency of the developed models.

Acknowledgements

The work reported here is carried out within ITOOL ('Integrated Tool for Simulation of Textile Composites') project funded by the European Commission. Ms Solange Amouroux and Mr Arnaud Alix (Dassault Aviation, France) are gratefully acknowledged for supplying the composite material. Authors would also like to thank Mr Kris van de Staey and Mr Paul Crabbé (Department of Metallurgy and Materials Engineering, K.U.Leuven) for assistance with the mechanical testing and polishing equipment.

References

1. B. T. Åström: 'Manufacturing of polymer composites'; 1997, London, Chapman & Hall.
2. V. Koissin, A. Ruopp, S. V. Lomov, I. Verpoest, V. Witzel and K. Drechsler: Proc. 12th Eur. Conf. on 'Composite materials', (eds. J. Lamon and A. T. Marques), (ECCM-12), Biarritz, France, August–September 2006, CD ROM.
3. V. Koissin, A. Ruopp, S. V. Lomov, I. Verpoest, V. Witzel and K. Drechsler: *Adv. Compos. Lett.*, 2006, **15**, (3), 87–94.
4. 'Priform UW 200 IMS G 24K 100 specification', Cytec Eng. Materials Inc., Wallingford, CT, USA, 2005.
5. 'Delivery programme and characteristics for Tenax filament yarn', Toho Tenax Europe GmbH, Wuppertal, Germany, 2008.
6. I. Verpoest and S. V. Lomov: *Compos. Sci. Technol.*, 2005, **65**, (15–16), 2563–2574.
7. V. Koissin, S. V. Lomov and I. Verpoest: Proc. 22nd Int. Conf. on 'Boundary and finite element methods', (ed. S. V. Lomov), (BEM-FEM-22), St. Petersburg, Russia, September 2007, CD ROM.
8. S. V. Lomov, G. Huysmans, Y. Luo, R. S. Parnas, A. Prodromou, I. Verpoest and F. R. Phelan: *Composites Part A*, 2001, **32A**, (10), 1379–1394.
9. H. Nakai, T. Kurashiki and M. Zako: Proc. 16th Int. Conf. on 'Composite materials', (ed. T. Ishkawa), (ICCM-16), Kyoto, Japan, July 2007, CD ROM.
10. H. Heß, Y. C. Roth and N. Himmel: *Compos. Sci. Technol.*, 2007, **67**, (6), 1081–1095.
11. U. Beier, F. Fischer, J. K. W. Sandler, V. Altstädt, C. Weimer and W. Buchs: *Composites Part A*, 2007, **38A**, 1655–1663.